XLVI CILAMCE
VITÓRIA - ES - BRAZIL - 2025
XLVI IBERO-LATIN AMERICAN CONGRESS ON COMPUTATIONAL METHODS IN ENGENEERING

Bubble deformation and breakup in shear flow: A Shan–Chen multicomponent LBM approach

Juan Felipe Aristizabal Aldana[1], Luiz Adolfo Hegele Junior[1]

[1]*Department of Petroleum Engineering, State University of Santa Catarina*
Avenida Lourival Cesário Pereira, 88336-275, Santa Catarina, Brazil
juan.aldana@edu.udesc.br, luiz.hegele@udesc.br

Abstract.

Bubble deformation and breakup under shear flow is a phenomenon that needs to be understood in order to mitigate oil spills using mechanical dispersant. This study presents a numerical investigation using the Lattice Boltzmann Method (LBM) with a multicomponent Shan–Chen pseudopotential model coupled with the regularized BGK (RBGK) collision operator, Guo's forcing Scheme and regularized boundary conditions (RBC). A two-dimensional domain lattice nodes is used with a shear flow inlet. The implementation focuses on Reynolds numbers ranging from 10 to 7000 while maintaining a fixed shear rate. The regularization approach enhances numerical stability, effectively reducing spurious currents compared to the standard BGK model. Initial results show that the bubble evolves from a stable shape into elongated forms and eventually breaks up, exhibiting patterns similar to bag or thick-rim bag breakup. These results validate the model's capability in capturing interface deformation and suggest a strong potential for future extensions to three-dimensional and high Reynolds number simulations.

Keywords: Lattice Boltzmann method, Pseudopotential Shan-Chen model, Regularization, Bubble deformation, Shear flow

1 Introduction

In offshore oil and gas production, leaks from submarine pipelines can release gas–oil mixtures that rise rapidly to the surface, leading to several environmental impacts. Mechanical dispersant techniques apply shear flows to large bubbles, breaking them into smaller ones, which slows their ascent and enhances natural biodegradation processes. However, the optimization of such dispersion systems demands a quantitative understanding of bubble deformation and breakup under shearing flow conditions [1].

The currently studies of this topic, primarily rely on experimental approaches and traditional computational fluid dynamics methods (CFD), such as the Volume of Fluid method such as Kékési et al. [2] approach. In some cases, the Lattice Boltzmann Method (LBM) has also been employed, particularly using the Multi-Relaxation Time model [3].

The Lattice Boltzmann Method, combined with multicomponent approaches such as the Shan-Chen pseudopotential model [4] shows a relevant alternative due to its mesoscopic nature and simplicity in handling complex interfaces. However, the behavior and instabilities of the Shan–Chen model under conditions of high shear and deformation are still under investigation. Therefore, it is necessary not only simulate the physical phenomenon of bubble breakup but also critically assess the accuracy, stability, and physical consistency of the Shan–Chen framework in these conditions.

In this context, the bubble behavior under shear conditions is relevant for the study of mechanical dispersant, but also it provides insight into how the Shan-Chen model behaves and performs that could leads to the development of more accurate and robust models.

Wherefore, the present work propose the use of the multicomponet Shan–Chen pseudopotential, along with the Regularized Lattice BGK model collision operator [5], the Guo[6] forcing scheme to ensure the second-order time accuracy and consistency, and regularized boundary conditions[7]. Simulations will be performed in two dimensions with a D2Q9 lattice, exploring a shear rates and Reynolds numbers, aiming in characterize both the physical breakup process and the numerical behavior of the Shan–Chen model under mechanical dispersion condition.

2 Methodology

2.1 Lattice Boltzmann method

The classical lattice Boltzmann equation, which adopts the Bhatnagar-Gross-Krook collision operator [8, 9] is given by:

$$f_i(\mathbf{x} + \mathbf{c}_i\Delta t, t + \Delta t) = f_i(\mathbf{x}, t) + \frac{\Delta t}{\tau}\left(f_i^{eq}(\mathbf{x}, t) - f_i(\mathbf{x}, t)\right), \tag{1}$$

In that previous equation, $f_i(\mathbf{x}, t)$ denotes the discrete distribution function, which quantifies the likelihood of finding a particle at a given position $\mathbf{x}$ at time t, traveling with the discrete velocity $\mathbf{c}_i$. Using the discrete model D2Q9, $\mathbf{c}_i = 0, \ldots, 8$. The Δt represents the lattice time step. Furthermore, the parameter τ is the relaxation time, which governs the kinematic viscosity ν of the lattice fluid according to the following relation:

$$\nu = a_s^{-2}\left(\tau - \frac{1}{2}\Delta t\right). \tag{2}$$

Besides, the left-hand side of the Equation (1) represents the propagation, also known as the free streaming of particles along the lattice in the direction dictated by $\mathbf{c}_i$. The right-hand side captures the collisional dynamics, driving the distribution functions toward their corresponding local equilibrium distributions [10]. That equilibrium function f_i^{eq} is a Maxwell-Boltzmann distribution of the fluid velocities at low Mach number [5] and it arises from a second-order velocity expansion in Hermite polynomials [11] that can be expanded as:

$$f_i^{eq}(\mathbf{x}, t) = w_i\rho\left(1 + a_s^2\, u_\alpha\, \mathbf{c}_{i\alpha} + \frac{1}{2}a_s^4\, u_\alpha u_\beta\, \mathscr{H}^{(2)}_{\alpha\beta,i}\right). \tag{3}$$

Here, a_s is defined as $a_s = 1/c_s$, where $c_s = \sqrt{3}$ denotes the lattice speed of sound. The vector u represents the macroscopic velocity field. In addition, $\mathscr{H}^{(2)}_{\alpha\beta,i}$ is the second-order Hermite tensor, given by $c_{i\alpha}c_{i\beta} - a_s^{-2}\delta_{\alpha\beta}$, and $\delta_{\alpha\beta}$ is the Kronecker delta. The terms w_i correspond to the quadrature weights used in defining the discrete equilibrium distribution functions.

The hydrodynamic quantities such as density, linear momentum, and the second order moment can be derived from the set of particle distribution functions by performing suitable weighted summations:

$$\rho = \sum_i f_i, \quad \rho u_\alpha = \sum_i f_i c_{i\alpha}, \quad \rho m^{(2)}_{\alpha\beta} = \sum_i f_i \mathscr{H}^{(2)}_{\alpha\beta,i}. \tag{4}$$

Subsequently, if the distribution function f_i is expanded in Taylor series using the terms of the Knudsen number parameter ϵ such as $f_i = f_i^{(0)} + \epsilon f_i^{(1)} + \epsilon^2 f_i^{(2)} + \ldots$, a Chapman-Enskog analysis [12], reveals that at zeroth order in ϵ, $f_i^{(0)} = f_i^{\text{eq}}$. This condition leads to the following equation proposed in the Latt and Chopard [5], Higuera et al. [13] articles:

$$f_i = f_i^{\text{eq}} + f_i^{\text{neq}}. \tag{5}$$

From this point, it can be assumed that only the two lower order terms in the Knudsen number expansion, can fully recover the Navier–Stokes equations and capture the complete physical dynamics. Therefore the first order in ϵ, $f_i^{(1)} = f_i^{\text{neq}}$, while the higher-order terms are neglected. Through the Chapman–Enskog analysis, an explicit expression for the non-equilibrium distribution $\hat{f}_i^{\text{neq}}$ is obtained:

$$\hat{f}_i^{\text{neq}}(\mathbf{x}, t) = \frac{1}{2}\rho w_i a_s^4\left(m^{(2)}_{\alpha\beta} - u_\alpha u_\beta\right)\mathscr{H}^{(2)}_{\alpha\beta,i}. \tag{6}$$

Moreover, using the early lattice Boltzmann formulations in matrix form [10], The regularized BGK (RBGK) can be written as:

$$f_i(\mathbf{x} + \mathbf{c}_i\Delta t, t + \Delta t) = f_i^{eq}(\mathbf{x}, t) + (1 - \omega)\,\hat{f}_i^{\text{neq}}(\mathbf{x}, t). \tag{7}$$

Where, $\omega = 1/\tau$. This formulation removes all unwanted modes (ghost modes) from the distribution function, retaining only the relevant hydrodynamic components, namely, the conserved and transport modes being the key principle of the RBGK model. Furthermore, highlighting an often unnoticed concept, the regularized model can be interpreted as a simplified variant of the multi-relaxation-time (MRT) model [14, 15], effectively employing two relaxation rates. In contrast the conventional BGK model present in the Equation (1), all non-equilibrium moments relax toward equilibrium using a single relaxation time (τ). This RBGK model introduces two relaxation scales, one governed by ω, which controls the physical transport processes such as viscosity, and another implicit scale that instantaneously suppresses the ghost modes equivalently relaxed with $\omega = 1$.

Note that, with the regularization of the non-equilibrium component $\hat{f}_i^{\,\text{neq}}$, Equation (5) becomes the sum of the equilibrium part f_i^{eq} and the regularized non-equilibrium part $\hat{f}_i^{\,\text{neq}}$, resulting in the regularized distribution function $\hat{f}_i$, which can be expressed as:

$$\hat{f}_i(\mathbf{x}, t) = \rho w_i \left(1 + a_s^2\, u_\alpha c_{i\alpha} + \frac{1}{2} a_s^4\, m^{(2)}_{\alpha\beta} \mathscr{H}^{(2)}_{\alpha\beta,i}\right). \tag{8}$$

2.2 Multicomponent Shan-Chen model

On the other hand, this work propose shear bubbles with different Reynolds rate using water as shearing flow and an air bubble, resulting in two components. Exist several approaches to simulate the interaction behavior between different fluids such as top-down approaches as the Free-Energy Method [16] and another methods with bottom-up approaches such as Color-Gradient [17] and Shan-Chen Pseudopotential Method [4, 18]. In this particularly case, the Shan-Chen (SC) model is chosen as the interaction model, owing to its inherent simplicity and its mesoscopic character. In the SC method, the surface tension naturally emerges as an effective outcome rather than being explicitly imposed. This behavior is analogous to the essence of the Lattice Boltzmann Method itself, which relies on simple mesoscopic dynamics to produce emergent macroscopic transport properties, such as fluid viscosity. Furthermore, in this multicomponent formulation, each distinct set of particle populations directly represents a different fluid component, offering physically transparent way to model multicomponent systems [19].

The SC model mimics the intermolecular forces between each fluid. These forces act between pairs of molecules and are additive. As a result, regions with higher molecular density experience stronger interaction forces. Therefore, the interaction force between two fluid elements at $\mathbf{x}$ and $\tilde{\mathbf{x}}$ is proportional to $\rho(\mathbf{x})\,\rho(\tilde{\mathbf{x}})$ and strongly depends on their distance. This dependence is captured by a function known as the kernel function $G(\mathbf{x}, \tilde{\mathbf{x}})$. The total force at $\mathbf{x}$ is obtained by integrating over all neighboring sites, leading to the following expression [4]:

$$\mathbf{F}^{SC}(\mathbf{x}) = -\int (\tilde{\mathbf{x}} - \mathbf{x})\, G(\mathbf{x}, \tilde{\mathbf{x}})\, \psi(\mathbf{x})\, \psi(\tilde{\mathbf{x}})\, \mathrm{d}^3\tilde{\mathbf{x}}. \tag{9}$$

For practical and stability reasons, ρ is replaced by an effective density function ψ, known as the pseudopotential, and is given by:

$$\psi(\rho) = \rho_0 \left(1 - e^{-\rho/\rho_0}\right). \tag{10}$$

Where ρ_0 is the reference density. Thus, the Equation (9) can be discretised in the following way:

$$\mathbf{F}^{SC(\sigma)}(\mathbf{x}) = -\psi^{(\sigma)}(\mathbf{x}) \sum_{\tilde{\sigma} \neq \sigma} G_{\sigma\tilde{\sigma}} \sum_i w_i\, \psi^{(\tilde{\sigma})}(\mathbf{x} + \mathbf{c}_i \Delta t)\, \mathbf{c}_i\, \Delta t. \tag{11}$$

Where the coefficient $G_{\sigma\tilde{\sigma}}$ collapses into a scalar number that controls the strength of the interaction, it is attractive for negative and repulsive for positive values. Here, $G_{\sigma\tilde{\sigma}} = G_{\tilde{\sigma}\sigma}$, with $\tilde{\sigma} \neq \sigma$, denotes the molecular interactions between different fluid components.

Highlighting that, in single-component systems, for $f_i^{eq,\sigma}$ the density must be ρ^σ, and the velocity must be replaced by $\mathbf{u}^\sigma$. Currently, for multicomponent fluids, ρ^σ is correctly used in $f_i^{eq,\sigma}$, but it is not clear which velocity should be used in the equilibrium functions since multiple sets of populations are present. For this reason, Sega et al. 20 derived an algorithm in which, for all component equilibrium functions, the velocity must be replaced by the barycentric velocity.

$$\mathbf{u}^{eq(\sigma)} = \mathbf{u}_b = \frac{1}{\rho}\sum_{\sigma}\left(\sum_i f_i^{(\sigma)}\mathbf{c}_i + \frac{\mathbf{F}^{SC(\sigma)}\Delta t}{2}\right), \quad \rho = \sum_{\sigma}\rho^{(\sigma)}. \tag{12}$$

Where the barycentric velocity is force-corrected to achieve second-order time accuracy, while the force expansion in Hermite polynomials truncated at second order gives:

$$F_i^{(\sigma)} = w_i\left(a_s^2\, c_{i\alpha} + a_s^4\, u_\beta\, \mathscr{H}^{(2)}_{\alpha\beta,i}\right) F_\alpha{}^{SC(\sigma)}. \tag{13}$$

Moreover the velocity moments for the force are given by:

$$\sum_i F_i = 0, \qquad \sum_i F_i\, c_{i\alpha} = F_\alpha, \qquad \sum_i F_i\, \mathscr{H}^{(2)}_{\alpha\beta,i} = F_\alpha u_\beta + F_\beta u_\alpha. \tag{14}$$

Therefore, applying the Guo forcing scheme [6, 21], the lattice Boltzmann equation (1) transforms into:

$$f_i{}^{(\sigma)}(\mathbf{x}+\mathbf{c}_i\Delta t, t+\Delta t) = f_i^{eq\,(\sigma)}(\mathbf{x},t) + \frac{\Delta t}{\tau}\left(f_i^{eq\,(\sigma)}(\mathbf{x},t) - f_i{}^{(\sigma)}(\mathbf{x},t)\right) + \left(1-\frac{\Delta t}{2\tau^{(\sigma)}}\right) F_i^{(\sigma)}(\mathbf{x},t). \tag{15}$$

Accordingly, the first order moment requires modification in order to incorporate the contribution of the external force, in the following way:

$$\rho^{(\sigma)}u_\alpha^{(\sigma)} = \sum_i f_i^{(\sigma)}c_{i\alpha} + \frac{\Delta t}{2}\sum_i F_i^{(\sigma)}. \tag{16}$$

With the above equation, it is now possible to determine the velocity for each component separately. Furthermore, by considering the new LBM Equation (15), that incorporates the force term and applying the Chapman-Enskog analysis, it can be derivative the expression for the non-equilibrium distribution function $\hat{f}_i^{\,\text{neq}}$, which is given by:

$$\hat{f}_i^{\text{neq}}(\mathbf{x},t) = \frac{1}{2}\rho w_i a_s^4\left(m^{(2)}_{\alpha\beta} - u_\alpha u_\beta\right)\mathscr{H}^{(2)}_{\alpha\beta,i} + w_i\frac{\Delta t\, a_s^4}{4}\left(F_\alpha u_\beta + F_\beta u_\alpha\right)\mathscr{H}^{(2)}_{\alpha\beta,i} - \frac{\Delta t}{2}F_i. \tag{17}$$

Thus, according to Equation (7) and the Equation (15), the regularized lattice Boltzmann equation can be written as:

$$f_i{}^{(\sigma)}(\mathbf{x}+\mathbf{c}_i\Delta t, t+\Delta t) = f_i^{eq\,(\sigma)}(\mathbf{x},t) + (1-\omega)\,\hat{f}_i^{\,\text{neq}\,(\sigma)}(\mathbf{x},t) + \left(1-\frac{\Delta t}{2\tau^{(\sigma)}}\right) F_i^{(\sigma)}(\mathbf{x},t). \tag{18}$$

To conclude this section, by revisiting Equation (5) and substituting the regularized non-equilibrium distribution function $\hat{f}_i^{\,\text{neq}}$, it is possible to derive the homologous form of the regularized distribution function $\hat{f}_i$ present in the Equation (8), incorporating the effects of the force terms:

$$\hat{f}_i(\mathbf{x},t) = \rho w_i\left(1 + a_s^2\, u_\alpha c_{i\alpha} + \frac{1}{2}a_s^4\, m^{(2)}_{\alpha\beta}\mathscr{H}^{(2)}_{\alpha\beta,i}\right) + w_i\frac{\Delta t\, a_s^4}{4}\left(F_\alpha u_\beta + F_\beta u_\alpha\right)\mathscr{H}^{(2)}_{\alpha\beta,i} - \frac{\Delta t}{2}F_i. \tag{19}$$

2.3 Boundary conditions

Continue with this work, it is necessary to define the boundary conditions. For that purpose, the computational domain where the bubble is sheared is defined as a rectangular grid of 128×512 lattice nodes. A Dirichlet boundary condition is applied at the top (North) and bottom (South), where both boundaries are treated as solid walls with zero velocity in both the x and y components. On the other hand, the left boundary or inlet (West) is also subject to a Dirichlet boundary condition, but with a prescribed velocity. Periodic boundary conditions is applied to the top (North), bottom (South), and East boundaries. On the left boundary, a Dirichlet condition is imposed, where the velocity is prescribed. Finally, the right boundary or outlet (East) is assigned a Neumann boundary condition.

The two components of the prescribed velocity are such that the y component (u_y) is set to zero, while the x component (u_x) is defined as the superposition of a constant velocity u_0 and a symmetric shear, given by $u_x(y) = u_0 + G(y - y_0)$, where G is the shear rate and y_0 is the vertical coordinate of the droplet center.

Taking into account the objective of this study is evaluate the Shan–Chen model using the regularized LBM framework, and to analyze the deformation and breakup of a droplet under fully developed flows, the entire water component is initialized with the symmetric shear profile. This ensures that the flow field is already developed from the first time step, eliminating transient effects and allowing for a direct observation of the droplet dynamics under shear [2]. A overview of the boundary conditions is showed in the Figure 1.

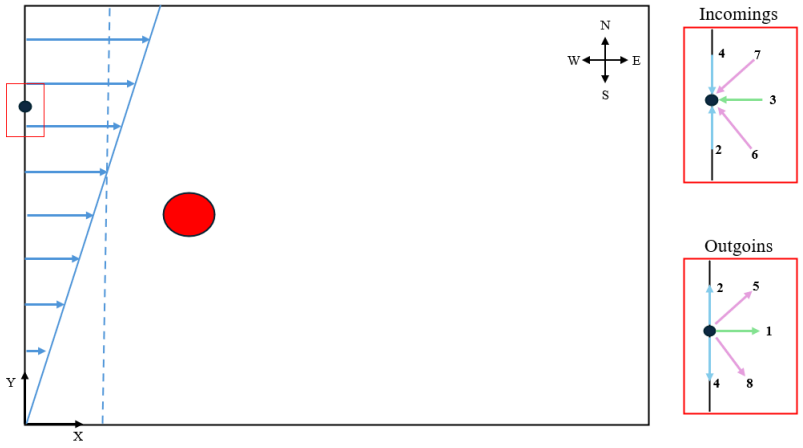


Figure 1. Boundary conditions with the incoming and outgoing populations at a west-side lattice node.

In this work, the regularized boundary conditions is implemented, following the framework proposed by Hegele et al. [7]. The method consists of summing the known and unknown regularized populations and subsequently computing the second-order moment:

$$\sum_{i\in I_s} f_i\,\mathscr{H}^{(2)}_{\alpha\beta,i} + \sum_{i\notin I_s} \hat{f}_i\,\mathscr{H}^{(2)}_{\alpha\beta,i} = \rho\, m^{(2)}_{\alpha\beta}. \tag{20}$$

Therefore, considering the incoming populations, gives the following equations:

$$\rho_I = \sum_{i\in I_s} \hat{f}_i, \qquad \rho_I m^{(2)}_{\alpha\beta,I} = \sum_{i\in I_s} \hat{f}_i\,\mathcal{H}^{(2)}_{\alpha\beta,i}. \tag{21}$$

And lastly, in order to close the system of equations, the conservation of mass during the collision step can be computed either as strong conservation of mass or weak conservation of mass, respectively, as follows:

$$\sum_{i\in I_s} f_i = \sum_{i\in O_s} \left((1-w)\,\hat{f}_i + w\, f^{\text{eq}}_i + \left(1-\frac{\Delta t}{2\tau}\right) F_i\right), \qquad \sum_{i\in I_s} f_i = \sum_{i\in I_s} \hat{f}_i \tag{22}$$

To implement the above Equations, it is necessary to define the incoming and outgoing directions. As an illustration, the inlet boundary condition will be determinate. As shown in Figure 1, the incoming populations (leaving the domain) and the outgoing populations (entering the domain) can be identified, and are composed by $I_s = \{0, 2, 3, 4, 6, 7\}$ and $O_s = \{0, 1, 2, 4, 5, 8\}$. Therefore, rearranging the Equation (21) and using the weak conservation Equation (22), is obtained the density and moments of the outgoing populations:

$$\rho^* = \frac{(4+3m_{xx_I})\rho_I}{3-3u_x}, \quad m^*_{xx} = \frac{9m_{xx_I}\rho_I + \rho + 3u_x\rho}{6\rho}, \quad m^*_{yy} = \frac{6m_{yy_I}\rho_I}{5\rho}, \quad m^*_{xy} = \frac{2m_{xy_I}\rho_I}{\rho}. \tag{23}$$

Accordingly, $\hat{f}^{\text{out}}(\rho^*, m^*_{xx}, m^*_{xy}, m^*_{yy})$ can be computed, and therefore the whole inlet boundary. Similarly, the remaining boundary conditions can be derived following the same procedure.

3 Results and discussion

Following the theoretical foundations discussed in the previous sections and implementing these concepts into a homemade code, a stable bubble was successfully obtained, as shown in the Figure 2, using a grid of 32×32 lattice nodes. Although the bubble remains stable throughout the entire simulation, it is important to highlight

that during the initial time steps, the bubble underwent oscillations, where initially shrinking and subsequently expanding, converging into a stable shape after a brief transient period. In addition, when the velocity field is plotted as arrows over the density field, small eddies appear around the bubble together with additional velocities at the water–air interface. These are commonly referred to as spurious velocities [22–24].

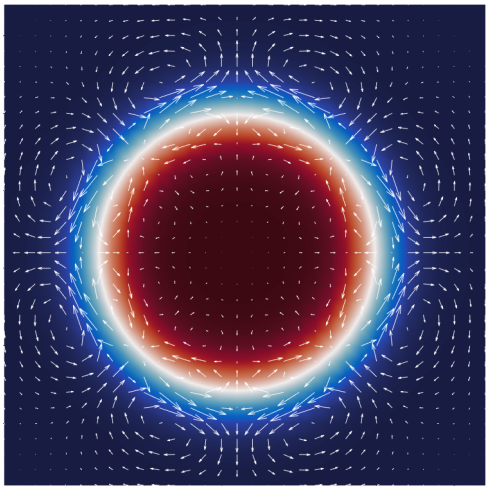


Figure 2. Stable initial bubble in the absence of shear flow, showing the presence of spurious velocities.

Subsequently, based on the imposed shear flow and boundary conditions, the water flow approximates the desired shear profile. This occurs because the top boundary is treated as a wall, preventing the upper layers from reaching the maximum velocity at the top. The wall effect reduces the velocity near the boundary to nearly zero, although it does not significantly affect the overall simulation. The Figure 3 illustrates the velocity field corresponding to the imposed shear flow profile.



Figure 3. Velocity field illustrating the shear flow at Reynolds 7000, $t = 2300$.

Several Reynolds numbers were considered, ranging from 10 to 7000. Similar behaviors were observed across all Reynolds numbers, identifying a case of bag breakup or possibly thick rim bag breakup, according to Kékési et al. [2]. Since the shear rate G was not varied, some of these results can be seen in Figure 4.

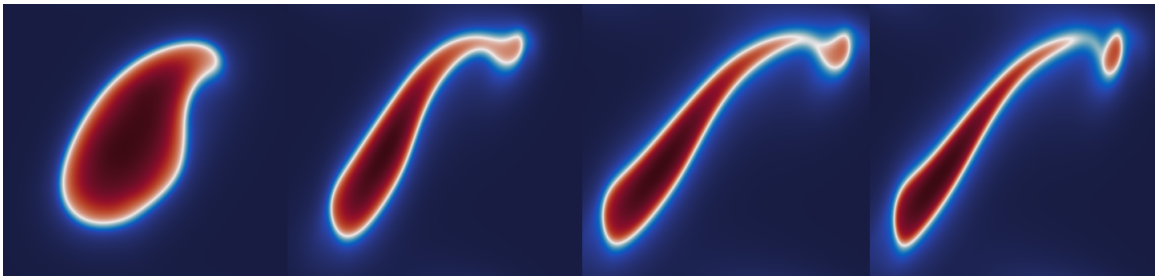


Figure 4. Bubble deformation and breakup at Reynolds 7000, $t = 600, 1700, 2300$, and 2700.

4 Conclusion

In this implementation, the Shan–Chen model was approached from a less conventional perspective by employing the regularized BGK collision operator instead of the commonly used MRT scheme. Highlighting that the model exhibited good stability under the applied Reynolds numbers, as the bubble did not collapse or produce unphysical values tending toward infinity. Furthermore, another indication of the model's stability is observed when the bubble is in stationary state (without presence of shear flow), exhibiting only minimal spurious currents significantly fewer than those typically observed with the non-regularized BGK model [19].

Moreover, the oscillations observed in the initially stationary bubble can be attributed to physical effects. These arise since the initial conditions are typically not in equilibrium with the Shan-Chen pseudopotential forces. As a result, there is a pressure imbalance between the inside and outside of the bubble, which leads into transient mass fluxes and leads to the observed expansion and contraction during the early stages of the simulation.

In the simulations, Reynolds numbers ranging from 10 to 7000 were tested, all of which remained stable without causing the simulations to collapse. However, during the initial stages of the simulations, the regions surrounding the bubble exhibited unphysical velocity values, which exceeded the imposed shear flow velocity. This behavior introduced transient instabilities at the beginning of the simulations. After several time steps, these velocities around the bubble gradually decreased. Moreover, it was not possible to perform simulations at higher Reynolds numbers due to the same instability issue near the bubble. Despite these limitations, two possible shear-induced breakup modes were identified: bag breakup and possibly thick-rim bag breakup. The bubble was observed to elongate progressively until reaching a critical point where it was sheared apart. Nevertheless, future work aims to implement modifications to the Shan–Chen model to mitigate these unphysical velocities, enabling more accurate simulations and improving the understanding of bubble breakup dynamics, ultimately contributing to the optimization of mechanical dispersant.

Finally work was implemented using the D2Q9 lattice Boltzmann model on CPU, with the aim of understanding the method's behavior and evaluating its performance using the regularized lattice Boltzmann approach. Nevertheless, future work is expected to extend this implementation to the D3Q27 model using GPU acceleration, following recent advances in high-performance computing LBM frameworks such as those proposed by Montessori et al. [25].

Acknowledgements.

The authors gratefully acknowledge the academic support provided by the Master's Program in Mechanical Engineering at the Santa Catarina State University (UDESC). Additionally, the first author wishes to acknowledge the financial support from the Foundation for the Support of Research and Innovation of the State of Santa Catarina (FAPESC).

Authorship statement. The authors hereby confirm that they are the sole liable persons responsible for the authorship of this work, and that all material that has been herein included as part of the present paper is either the property (and authorship) of the authors, or has the permission of the owners to be included here.

References

[1] Ø. Johansen, H. Rye, and C. Cooper. Deepspill—field study of a simulated oil and gas blowout in deep water. *Spill Science Technology Bulletin*, vol. 8, n. 5–6, pp. 433–443, 2003.

[2] T. Kékési, G. Amberg, and L. P. Wittberg. Drop deformation and breakup in flows with shear. *Chemical Engineering Science*, vol. 140, pp. 319–329, 2016.

[3] J. Zhang, H. Chen, Y. Zhou, and G. Cao. Simulation on the process of single bubble floating and colliding oil droplet based on improved three-component pseudo-potential boltzmann method. *Journal of Petroleum Science and Engineering*, vol. 198, pp. 108119, 2021.

[4] X. Shan and H. Chen. Lattice boltzmann model for simulating flows with multiple phases and components. *Physical Review E*, vol. 47, n. 3, pp. 1815–1819, 1993.

[5] J. Latt and B. Chopard. Lattice boltzmann method with regularized pre-collision distribution functions. *Mathematics and Computers in Simulation*, vol. 72, pp. 165–168, 2006.

[6] Z. Guo, C. Zheng, and B. Shi. Discrete lattice effects on the forcing term in the lattice boltzmann method. *Physical Review E*, vol. 65, pp. 046308, 2002.

[7] L. A. Hegele, A. Scagliarini, M. Sbragaglia, K. K. Mattila, P. C. Philippi, D. F. Puleri, J. Gounley, and A. Randles. High-reynolds-number turbulent cavity flow using the lattice boltzmann method. *Physical Review E*, vol. 98, n. 4, pp. 043302, 2018.

[8] S. Succi. *The Lattice Boltzmann Equation for Fluid Dynamics and Beyond*. Oxford University Press, 2001.
[9] P. L. Bhatnagar, E. P. Gross, and M. Krook. A model for collision processes in gases. i. small amplitude processes in charged and neutral one-component systems. *Physical Review*, vol. 94, n. 3, pp. 511–525, 1954.
[10] A. Montessori, G. Falcucci, P. Prestininzi, M. L. Rocca, and S. Succi. Regularized lattice bhatnagar-gross-krook model for two- and three-dimensional cavity flow simulations. *Physical Review E*, vol. 89, n. 5, pp. 053317, 2014.
[11] H. Grad. Note on n-dimensional hermite polynomials. *Communications on Pure and Applied Mathematics*, vol. 2, n. 4, pp. 325–330, 1949.
[12] S. Chapman and T. G. Cowling. *The Mathematical Theory of Non-uniform Gases: An Account of the Kinetic Theory of Viscosity, Thermal Conduction, and Diffusion in Gases*. Cambridge University Press, Cambridge, 2 edition, 1952.
[13] F. J. Higuera, S. Succi, and R. Benzi. Lattice gas dynamics with enhanced collisions. *Europhysics Letters*, vol. 9, n. 4, pp. 345–349, 1989.
[14] P. Asinari. Multiple-relaxation-time lattice boltzmann scheme for homogeneous mixture flows with external force. *Physical Review E*, vol. 77, n. 5, pp. 056706, 2008.
[15] D. d'Humières. Generalized lattice boltzmann equations. *Rarefied Gas Dynamics: Theory and Simulations, Progress in Astronautics and Aeronautics*, vol. 159, pp. 450–458, 1992.
[16] M. R. Swift, W. R. Osborn, and J. M. Yeomans. Lattice boltzmann simulation of nonideal fluids. *Physical Review Letters*, vol. 75, n. 5, pp. 830–833, 1995.
[17] A. K. Gunstensen, D. H. Rothman, S. Zaleski, and G. Zanetti. Lattice boltzmann model of immiscible fluids. *Physical Review A*, vol. 43, n. 8, pp. 4320–4327, 1991.
[18] X. Shan and G. Doolen. Multicomponent lattice-boltzmann model with interparticle interaction. *Journal of Statistical Physics*, vol. 81, n. 1-2, pp. 379–393, 1995.
[19] T. Krüger, H. Kusumaatmaja, A. Kuzmin, O. Shardt, G. Silva, and E. M. Viggen. *The Lattice Boltzmann Method: Principles and Practice*. Springer, 2017.
[20] M. Sega, M. Sbragaglia, S. S. Kantorovich, and A. O. Ivanov. Mesoscale structures at complex fluid-fluid interfaces: a novel lattice boltzmann / molecular dynamics coupling. *Soft Matter*, vol. 9, n. 42, pp. 10092–10101, 2013.
[21] G. Silva and V. Semião. First- and second-order forcing expansions in a lattice Boltzmann method reproducing isothermal hydrodynamics in artificial compressibility form. *Journal of Fluid Mechanics*, vol. 698, pp. 282–303, 2012.
[22] A. J. Wagner. The origin of spurious velocities in lattice boltzmann. *International Journal of Modern Physics B*, vol. 17, n. 1–2, pp. 193–196, 2003.
[23] K. Connington and T. Lee. A review of spurious currents in the lattice Boltzmann method for multiphase flows. *Journal of Mechanical Science and Technology*, vol. 26, n. 12, pp. 3857–3863, 2012.
[24] D. P. F. Silva, R. C. V. Coelho, da M. M. T. Gama, and N. A. M. Araújo. Effect of droplet deformability on shear thinning in a cylindrical channel. *Physical Review E*, vol. 107, n. 3, pp. 035106, 2023.
[25] A. Montessori, M. L. Rocca, G. Amati, M. Lauricella, A. Tiribocchi, and S. Succi. High-order thread-safe lattice boltzmann model for hpc turbulent flow simulations, 2024.